Kinetic Control of Multiple Forms of Ca^{2+} Spikes by Inositol Trisphosphate in Pancreatic Acinar Cells

Koichi Ito, Yasushi Miyashita, and Haruo Kasai

Department of Physiology, Faculty of Medicine, University of Tokyo, Hongo, Bunkyo-ku, Tokyo 113-0033, Japan

Abstract. The mechanisms of agonist-induced Ca^{2+} spikes have been investigated using a caged inositol 1,4,5-trisphosphate (IP_3) and a low-affinity Ca^{2+} indicator, BTC, in pancreatic acinar cells. Rapid photolysis of caged IP_3 was able to reproduce acetylcholine (ACh)-induced three forms of Ca^{2+} spikes: local Ca^{2+} spikes and submicromolar (<1 μM) and micromolar (1–15 μM) global Ca^{2+} spikes (Ca^{2+} waves). These observations indicate that subcellular gradients of IP_3 sensitivity underlie all forms of ACh-induced Ca^{2+} spikes, and that the amplitude and extent of Ca^{2+} spikes are determined by the concentration of IP_3. IP_3-induced local Ca^{2+} spikes exhibited similar time courses to those generated by ACh, supporting a role for Ca^{2+}-induced Ca^{2+} release in local Ca^{2+} spikes. In contrast, IP_3-induced global Ca^{2+} spikes were consistently faster than those evoked with ACh at all concentrations of IP_3 and ACh, suggesting that production of IP_3 via phospholipase C was slow and limited the spread of the Ca^{2+} spikes. Indeed, gradual photolysis of caged IP_3 reproduced ACh-induced slow Ca^{2+} spikes. Thus, local and global Ca^{2+} spikes involve distinct mechanisms, and the kinetics of global Ca^{2+} spikes depends on that of IP_3 production particularly in those cells such as acinar cells where heterogeneity in IP_3 sensitivity plays critical role.

Key words: Ca^{2+} waves • caged-IP_3 • Ca^{2+} spikes • secretion • inositol trisphosphate

AGONIST receptors induce the release of Ca^{2+} from intracellular stores and thereby generate Ca^{2+} spikes, waves, or oscillations that play important roles in many cellular functions (Berridge, 1993; Petersen et al., 1994; Clapham, 1995). It is thought that positive feedback effects of Ca^{2+} on Ca^{2+}-release channels, including both inositol 1,4,5-trisphosphate (IP_3)[1] (Iino, 1989; Bezprozvanny et al., 1991) and ryanodine receptors (Endo et al., 1970), result in Ca^{2+}-induced Ca^{2+} release (CICR) and contribute to the generation of such Ca^{2+} responses. Indeed, local Ca^{2+} release events induced by IP_3, such as puffs (Callamaras et al., 1998) and local Ca^{2+} spikes (Kasai et al., 1993; Thorn et al., 1993), are likely attributable to CICR mechanisms at IP_3 receptors, because they can be induced at constant concentrations of IP_3 (Wakui et al., 1989). However, it has remained unclear whether the generation of global Ca^{2+} spikes is also explained by CICR mechanisms (Bootman et al., 1997).

Address all correspondence to Dr. Haruo Kasai, Department of Physiology, Faculty of Medicine, University of Tokyo, Hongo, Bunkyo-ku, Tokyo 113-0033, Japan. Tel.: +81-3-5841-3460. Fax: +81-3-5841-3325. E-mail: hkasai@m.u-tokyo.ac.jp

1. *Abbreviations used in this paper:* ACh, acetylcholine; BTC, benzothiazole coumarin; $[Ca^{2+}]_i$, cytosolic Ca^{2+} concentration; CICR, Ca^{2+}-induced Ca^{2+} release; IP_3, inositol 1,4,5-trisphosphate; PLC, phospholipase C.

Pancreatic acinar cells represent an ideal system for investigating the mechanisms of agonist-induced generation of Ca^{2+} spikes. First, agonist-induced increases in the cytosolic concentration of Ca^{2+} ($[Ca^{2+}]_i$) in these cells are mostly attributable to the generation of IP_3 from phosphatidylinositol 4,5-bisphosphate in a reaction catalyzed by phospholipase C (PLC) (Petersen, 1992). Second, Ca^{2+} release channels are heterogeneously distributed along the polarized intracellular structures (Kasai et al., 1993), resulting in a fixed pattern of Ca^{2+} spike spread. The spikes are always initiated at the trigger zone, the apical pole of the secretory granule–containing region of the cell (Kasai and Augustine, 1990; Nathanson et al., 1992; Toescu et al., 1992). Thus, the functioning of distinct Ca^{2+}-release channels can be directly visualized. And third, agonists induce multiple forms of Ca^{2+} spikes in a dose-dependent manner; they can be local or global (Kasai et al., 1993; Thorn et al., 1993). Increases in $[Ca^{2+}]_i$ remain restricted to a discrete area or expand to entire cells in the local and global Ca^{2+} spikes, respectively. The global Ca^{2+} spikes further manifest at submicromolar or micromolar concentrations of Ca^{2+} (Ito et al., 1997). The existence of multiple forms of Ca^{2+} spikes in the acinar cells enables us to investigate their mechanisms in the same experimental conditions.

We have now characterized the Ca^{2+} spikes induced by spatially uniform and rapid increases in $[IP_3]_i$, generated

© The Rockefeller University Press, 0021-9525/99/07/405/9 $5.00

by photolysis of caged IP_3, and compared them with the Ca^{2+} spikes induced by a natural stimulus, acetylcholine (ACh). If CICR mechanisms play a dominant role in ACh-induced Ca^{2+} spikes, then the time course of such spikes should resemble that of those induced by IP_3. We found that this was indeed the case for local Ca^{2+} spikes, but not for global Ca^{2+} spikes. Ca^{2+} imaging was performed with a low-affinity Ca^{2+} indicator, benzothiazole coumarin (BTC), that minimizes the effects of changes in intrinsic Ca^{2+} buffering in the cells and allowed us to quantify large increases in $[Ca^{2+}]_i$ without the problem of dye saturation (Ito et al., 1997; Kasai and Takahashi, 1999).

Materials and Methods

Preparation of Acinar Cells

Acinar cells were dissociated from the pancreas of 5–7-wk-old mice by enzymatic treatment as described (Ito et al., 1997). For electrophysiological recording, the cells were dispersed in a small chamber in a solution (Sol A) containing 140 mM NaCl, 5 mM KCl, 2 mM $CaCl_2$, 1 mM $MgCl_2$, 10 mM Hepes-NaOH (pH 7.4), and 10 mM glucose. ACh (Wako) was dissolved in Sol A and applied to cells through a glass pipette. Ca^{2+} indicators, fluo-3 or BTC (Molecular Probes), were dissolved in a solution (basic internal solution) containing 120 mM cesium glutamate, 5 mM CsCl, 50 mM Hepes-CsOH (pH 7.2), 1 mM ATP, 0.2 mM GTP, and 2 mM $MgCl_2$, and were then loaded into cells at a concentration of 200 μM by the patch clamp method. Caged IP_3 [D-*myo*-inositol 1,4,5-trisphosphate, $P^{4(5)}$-1-(2-nitrophenyl)-ethyl ester; Calbiochem-Novabiochem] or caged $GPIP_2$ [1-(α-glycerophosphoryl)-D-*myo*-inositol 4,5-bisphosphate, $P^{4(5)}$-1-(2-nitrophenyl)-ethyl ester; Calbiochem-Novabiochem] was also added to the basic internal solution. Osmolarities of the external and internal solutions were estimated to be ~310 mOsM after addition of all chemicals (Semi-Micro Osmometer; Knauer). All experiments were performed under yellow light illumination (FL40S-Y-F; National) at room temperature (22–25°C).

Ca^{2+} Imaging

Confocal Ca^{2+} imaging was performed as described (Kasai et al., 1993), with the exception that fluo-3 was used as the Ca^{2+} indicator. Fluorescence from patch-clamped acinar cells was detected with a confocal laser scanning microscope (MRC-600; Bio-Rad) attached to an inverted microscope (IMT-2; Olympus) with an objective lens (DApo 40× UV/340 oil; Olympus). Fluo-3 was excited with an argon laser at 488 nm, and $[Ca^{2+}]_i$ was calculated from the ratio of fluorescence values during stimulation (F) to that obtained before stimulation (F_0) according to the equation

$$\left[Ca^{2+}\right]_i = K\frac{\dfrac{1+\left[Ca^{2+}\right]_0/K}{1+\left((F_{max}/F_{min})\left[Ca^{2+}\right]_0\right)/K} - F/F_0}{F/F_0 - \dfrac{1+\left[Ca^{2+}\right]_0/K}{(F_{min}/F_{max})+\left[Ca^{2+}\right]_0/K}}, \quad (1)$$

where K and $[Ca^{2+}]_0$ were assumed to be 0.39 and 0.1 μM, respectively. Values of F_{max}/F_{min} were estimated in vivo by assuming that the maximal $[Ca^{2+}]_i$ achieved in the presence of ACh (10 μM) was 10 μM (see Fig. 6, A and B). The mean value of F_{max}/F_{min} thus obtained was 6.5 and was used to calibrate local Ca^{2+} spikes induced with a low concentration of IP_3 (see Fig. 1 A).

Ca^{2+} imaging with a cooled CCD camera was performed as described (Ito et al., 1997). In brief, a recording chamber was placed on an inverted microscope (IX; Olympus) and observed through an objective lens (DApo 40× UV/340 oil). The $[Ca^{2+}]_i$ was measured with the Ca^{2+} indicator BTC. Monochromatic beams with wavelengths of 430 or 480 nm were isolated from light emitted by a xenon lamp with the use of a polychromator (T.I.L.L. Photonics), and were fed into one port of a light guide (IX-RFA caged; Olympus). The light was reflected by a dichroic mirror (DM500) placed beneath the objective lens, and fluorescent light emitted from the cells was captured with a cooled CCD camera system (T.I.L.L. Photonics) fixed at the side port of the microscope. The duration of image acquisition was 0.12 s, and the pairs of images were acquired every 0.24 s. $[Ca^{2+}]_i$ was estimated from BTC fluorescence as described (Ito et al., 1997). Calibration constants for BTC were $R_{max} = 2.0$ and $K_B\beta = 112$. To obtain Ca^{2+} images from BTC fluorescence, we first estimated the distribution of R_{min} in individual cells by averaging several frames of the resting distribution of R. This procedure was used to compensate for small heterogeneity in R_{min} within a cell, and to reduce noise levels, particularly at $[Ca^{2+}]_i$ values of <1 μM. The mean value of R_{min} ($m[R_{min}]$) was ~0.55. Distributions of ΔR were then calculated by subtracting the distribution of R_{min} from that of R. From ΔR, $[Ca^{2+}]_i$ was estimated as $K_B\beta\cdot\Delta R/(R_{max} - m[R_{min}] - \Delta R)$.

The $[Ca^{2+}]_i$ in Ca^{2+} images was represented by pseudocolor coding, where 0.1, 0.3, 1, 3, and 10 μM were expressed as blue, sky blue, green, yellow, and red, respectively (Figs. 1, 2, 3, and 6).

Photolysis of Caged IP_3

We used a mercury lamp (IX-RFC or IMT-2-RFC; Olympus) as an actinic light source for photolysis of caged IP_3. Light from the mercury lamp was filtered through a 360-nm band-pass filter and fed into the second port of the light guide (IX-RFA caged or IMT-2-RFC caged; Olympus). Incorporation of a dichroic mirror (DM400) allowed the light guide to accommodate two light sources, one for photolysis of IP_3 and the other for excitation of the Ca^{2+} indicator. Illumination from the actinic light was gated through an electric shutter (Copal). We estimated that irradiation for 125 ms was necessary and sufficient for full activation of caged IP_3. For this calibration experiment, the irradiation was restricted to a recorded cell and not applied to a patch pipette to facilitate recovery of $[IP_3]_i$ through the pipette, and photolysis was intermittently applied to the same cells. We found that Ca^{2+} responses depended on the duration of the irradiation, and reached the maximal response at 125 ms. In most experiments, we therefore set the duration of the opening of the shutter at 125 ms to achieve complete photolysis of caged IP_3, and the irradiation was applied to whole objective field including the tip of patch pipette to maintain $[IP_3]_i$ constant as long as possible. In some experiments, a neutral density filter (10, 20, or 50%) was used to reduce the light intensity, in which case the concentration of photolyzed IP_3 was obtained by multiplying the concentration of caged IP_3 introduced into the cells by the relative light intensity. Only those data obtained from the first photolysis were used to avoid complications of preceding Ca^{2+} spikes.

Results

IP_3-Induced Local Ca^{2+} Spikes

We first investigated whether homogeneous and constant increases in $[IP_3]_i$ could produce local Ca^{2+} spikes in the secretory granule area of pancreatic acinar cells similar to those induced by ACh. Photolysis of caged IP_3 was induced 2–5 min after the establishment of whole-cell perfusion, at which time the concentration of IP_3 in the cell should be equilibrated with that in the patch pipette. We monitored $[Ca^{2+}]_i$ with a confocal microscope and a high-affinity Ca^{2+} indicator dye, fluo-3. Local increases in $[Ca^{2+}]_i$ confined to small spots within the secretory granule area were detected immediately after photolysis of 5 μM caged IP_3 (Fig. 1 A). The spatial pattern of the IP_3-induced local Ca^{2+} spikes was similar to those induced by ACh (n = 7, data not shown; Kasai et al., 1993). The result is in accord with previous studies in which IP_3 was microinjected into the cells (Kasai et al., 1993; Thorn et al., 1993).

The time course of local Ca^{2+} spikes induced by photolysis of caged IP_3 (Fig. 1, A and B) also was similar to that of ACh-induced local Ca^{2+} spikes (Kasai et al., 1993). We believe that IP_3-induced Ca^{2+} spikes per se do not cause IP_3 production, because, in the absence of receptor stimulation, increases in $[Ca^{2+}]_i$ alone could not give rise to the

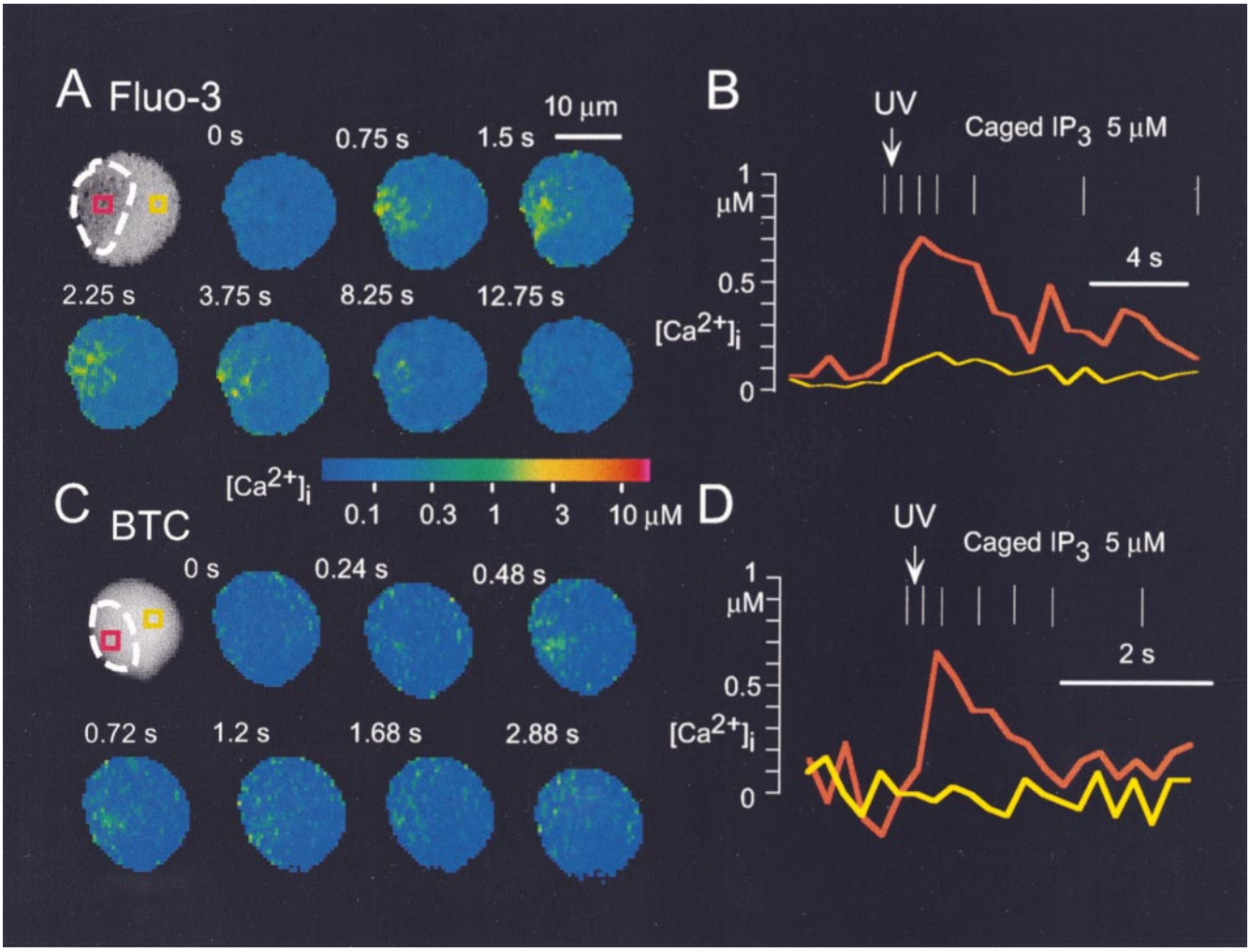

Figure 1. Local Ca^{2+} spikes induced by photolysis of caged IP_3 in pancreatic acinar cells. Local increases in $[Ca^{2+}]_i$ were induced by photolysis of 5 μM caged IP_3. (A) Ca^{2+} images obtained with a confocal microscope and the high-affinity Ca^{2+} indicator fluo-3. (B) Time courses of $[Ca^{2+}]_i$ within the rectangles shown in A. (C) Ca^{2+} images obtained with a cooled CCD camera and the low-affinity Ca^{2+} indicator BTC. (D) Time courses of $[Ca^{2+}]_i$ within the rectangles shown in C. Dashed white lines in the black and white photographs shown in A and C indicate the secretory granule region of the cell. Vertical white bars in B and D indicate the times when the images shown in A and C were obtained; the arrow indicates the time of photolysis of caged IP_3 induced by ultraviolet (UV) irradiation.

Ca^{2+} gradients characteristics of IP_3-induced Ca^{2+} spikes (Toescu et al., 1992; Maruyama et al., 1993). Thus, we believe that $[IP_3]_i$ stays constant during IP_3-induced Ca^{2+} spikes, and that local Ca^{2+} spikes were mediated by CICR mechanisms as reported (Wakui et al., 1989; Thorn et al., 1996). The increases in $[Ca^{2+}]_i$ were always transient in the experiments described in this study. The transient nature of the responses is likely attributable to desensitization of IP_3 receptors, given that photolyzed caged IP_3 was continuously perfused from the patch pipette and that a metabolically stable analogue of caged IP_3, caged $GPIP_2$, also induced transient increases in $[Ca^{2+}]_i$ ($n = 5$, data not shown). Concentrations of caged IP_3 of <1 μM did not trigger detectable increases in $[Ca^{2+}]_i$.

The local Ca^{2+} spikes also could be detected with the use of the low-affinity Ca^{2+} indicator BTC and a cooled CCD (charge-coupled device) camera (Fig. 1, C and D). A focal and transient increase in $[Ca^{2+}]_i$ of ~0.5 μM was detected in the trigger zone in response to photolysis of caged IP_3 ($n = 5$). The increases in $[Ca^{2+}]_i$ were confirmed by the appearance of Ca^{2+}-dependent Cl^- currents (data not shown). The detection of local Ca^{2+} spikes with BTC allowed us to make a direct comparison with their properties with those of global Ca^{2+} spikes recorded with BTC.

IP_3-Induced Global Ca^{2+} Spikes

We next examined the effects of rapid photolysis of larger concentrations of IP_3 (10–100 μM). Ratiometric Ca^{2+} imaging with BTC was used for reliable estimation of amplitudes and time courses of changes in $[Ca^{2+}]_i$ persisting for >20 s. Because of substantial cell-to-cell variability in the responses, these experiments were performed with a large number of cells ($n = 41$). Photolysis of 100 μM caged IP_3 often resulted in large increases in $[Ca^{2+}]_i$ throughout the cell that were apparent within 0.24 s (Fig. 2, A and B), the

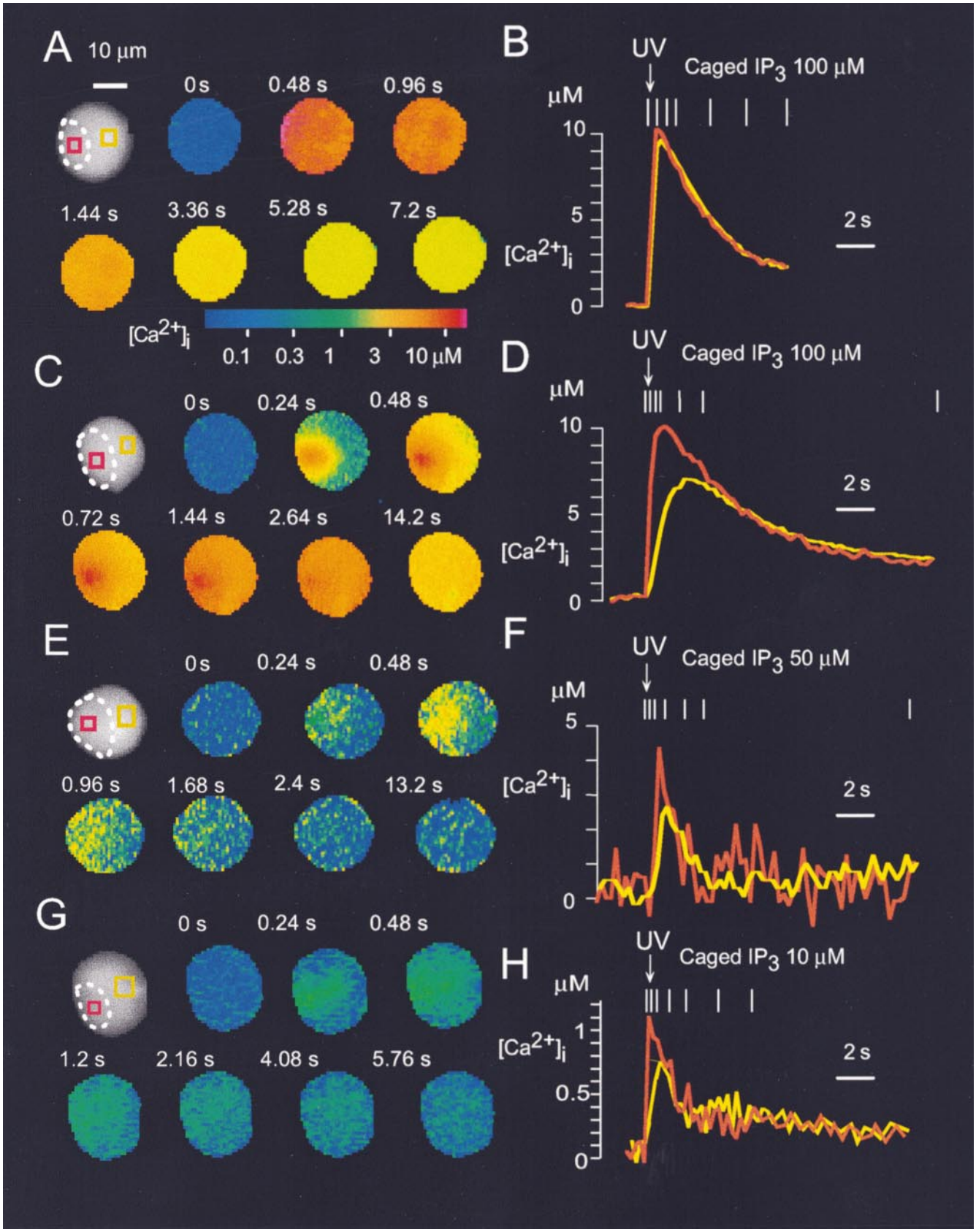

Figure 2. Global Ca^{2+} spikes or Ca^{2+} waves induced by photolysis of caged IP_3. (A and B) Homogeneous increase in $[Ca^{2+}]_i$ induced by photolysis of 100 μM caged IP_3. (C–H) Ca^{2+} waves induced by photolysis of 100 μM (C and D), 50 μM (E and F), or 10 μM (G and H) caged IP_3. Ca^{2+} images were obtained with a cooled CCD camera and BTC. Data are presented as described in the legend to Fig. 1.

earliest time at which an image was collected by the CCD camera. The Ca^{2+} indicator (BTC) was not saturated with Ca^{2+} at these concentrations (Fig. 2 A), and it can therefore be concluded that the increases in $[Ca^{2+}]_i$ were relatively homogeneous and exceeded 10 μM throughout the cell. Thus, the capacity for Ca^{2+} release appeared to be distributed homogeneously throughout the cell. The abundance of IP_3 receptors in the basal area was also supported by the previous observation that IP_3 injection could directly trigger Ca^{2+} release in the basal area (Fig. 6 C of Kasai et al., 1993).

Photolysis of caged IP_3 at concentrations between 10 and 100 μM induced Ca^{2+} spikes that were initiated at the trigger zone (Fig. 2, C, E, and G) as in the case with ACh-induced Ca^{2+} spikes. In fact, Ca^{2+} concentrations immediately (0.24 s) after photolysis of caged IP_3 were always larger in the trigger zone than in the basal area (Fig. 2, D, F, and H). Furthermore, the initial Ca^{2+} concentrations in the trigger zone (initial $[Ca^{2+}]_t$) and the basal area (initial $[Ca^{2+}]_b$) depended on $[IP_3]_i$ with median effective concentrations of 5 and 50 μM, respectively (Fig. 4, A and B). These data suggest that IP_3 receptors in the basal area were ~10 times less sensitive to IP_3 than those in the trigger zone. Gradual increases in $[Ca^{2+}]_i$ were detected throughout the cells after photolysis of caged IP_3, suggesting positive feedback effect of Ca^{2+} on Ca^{2+} release channels.

The peak amplitudes of the IP_3-induced Ca^{2+} spikes also depended on $[IP_3]_i$ (see Fig. 4 C), as those of ACh-induced Ca^{2+} spikes did on the concentration of ACh (see Fig. 4 D). The amplitudes of Ca^{2+} spikes ranged from micromolar, with concentrations of >10 μM in the trigger zone (Figs. 2 C and 3 A), to intermediate (~5 μM; Figs. 2 E and 3 C), to submicromolar (<1 μM) (Figs. 2 G and 3 E). The amplitudes of the smallest global Ca^{2+} spikes generated by IP_3 or ACh were <1 μM in most regions of the cell (Figs. 2 G and 3 E). The peak amplitudes of ACh-induced increases in $[Ca^{2+}]_i$ in the trigger zone were always larger than those in the basal area (Figs. 3 and 4 F). This Ca^{2+} gradient was not due to the gradient of $[IP_3]_i$, because similar Ca^{2+} gradients were induced by homogeneous increases in $[IP_3]_i$ induced by caged IP_3 (Figs. 2 and 4 E). Thus, IP_3 receptors in the basal area was less sensitive to IP_3 than those in trigger zone even at the peak of Ca^{2+} spikes in the respective areas.

Time Courses of Global Ca^{2+} Spikes

Marked differences were evident in the time courses of the global Ca^{2+} spikes induced by caged IP_3 and of those induced by ACh (Fig. 5). First, the time-to-peak for Ca^{2+} spikes at the trigger zone induced by caged IP_3 was <1 s in most experiments, and was independent of $[IP_3]_i$ (Fig. 5 A). In contrast, the time-to-peak for ACh-induced global Ca^{2+} spikes was >1 s in most experiments, and decreased as the concentration of ACh increased (Fig. 5 B). These data indicate that $[IP_3]_i$ increases gradually during ACh stimulation, and that the rate of this increase is dependent on ACh concentration.

Second, the spread of Ca^{2+} spikes induced by caged IP_3 was faster than that of those induced by ACh. To quantify the rate of spread of Ca^{2+} spikes (Ca^{2+} waves), we defined the spike spread time as the difference between the times at which the half-maximal $[Ca^{2+}]_i$ was achieved in the trigger zone and in the basal area. The spread time for spikes induced by caged IP_3 was <0.7 s in most experiments, and was independent of $[IP_3]_i$ ($P > 0.1$; Fig. 5 C). In contrast, the spread time for ACh-induced Ca^{2+} spikes was >0.7 s in most experiments, and it decreased as the concentration of ACh increased (Fig. 5 D).

Finally, the onset of Ca^{2+} spikes in the basal area was always delayed relative to that of Ca^{2+} spikes in the trigger zone for cells stimulated with ACh (Fig. 3), whereas little delay was observed for Ca^{2+} spikes induced by caged IP_3 (Fig. 2). We quantified the delay in the onset of Ca^{2+} spikes in the basal area by measuring the difference between the times at which $[Ca^{2+}]_i$ reached 0.5 μM in the trigger zone and in the basal area. The spike delay ranged between 0 and 0.24 s for IP_3-induced Ca^{2+} spikes (Fig. 5 E) and between 0.48 and 4 s for ACh-induced Ca^{2+} spikes (Fig. 5 F). Precise measurements of delay and spike spread times were not possible at high IP_3 concentrations with our cooled CCD camera operating at an acquisition interval of 0.24 s.

Line-Scan Analysis of Global Ca^{2+} Spikes

Therefore, we applied the line-scan mode of confocal laser scanning microscopy to analyze, in more detail, the speed of Ca^{2+} spikes (Ca^{2+} waves) induced by large concentrations of ACh (10 μM) or IP_3 (100 μM). We chose fluo-3 as the Ca^{2+} indicator for these experiments, because, unlike BTC, it was not excited by the ultraviolet light used for the activation of caged IP_3 and therefore permitted visualization of Ca^{2+} spikes during photolysis. The Ca^{2+} spikes induced by 10 μM ACh traversed the acinar cells with the spike spread time of 0.9 ± 1 s (mean ± SD, $n = 7$) and the spike delay of 0.9 ± 0.9 s (Fig. 6, A and B; Kasai et al., 1993), whereas those induced by 100 μM IP_3 exhibited the mean spread time of 0.1 ± 0.3 s ($n = 4$) and the delay of 0.1 ± 0.3 s (Fig. 6, C and D). These results were consistent with those obtained by two-dimensional imaging with BTC (Fig. 5). Thus, spread of ACh-induced Ca^{2+} spikes were consistently slower than those induced by rapid photolysis of caged IP_3 at all concentrations of IP_3 and ACh examined.

We postulated that the slow spread of ACh-induced Ca^{2+} spikes is due to slow generation of IP_3 and to sequential activation of Ca^{2+}-release channels with heterogeneous sensitivities for IP_3. To test this hypothesis, we reduced the rate of photolysis of caged IP_3 by decreasing the intensity of the actinic light source to 10% of its original value, so that the increase in $[IP_3]_i$ occurred over a period of 1 s. As predicted from our hypothesis, the spike spread time of the resulting Ca^{2+} spikes was increased to 0.7 ± 0.3 s ($n = 5$; Fig. 6, E and F). More importantly, the spike delay was also prolonged to 0.8 ± 0.3 s, similar to the spike delay for ACh-induced Ca^{2+} spikes (Fig. 6, A and B). Thus, an artificial slow increase in $[IP_3]_i$ was required to reproduce the time course of ACh-induced global Ca^{2+} spikes.

Discussion

We have demonstrated that spatially homogeneous in-

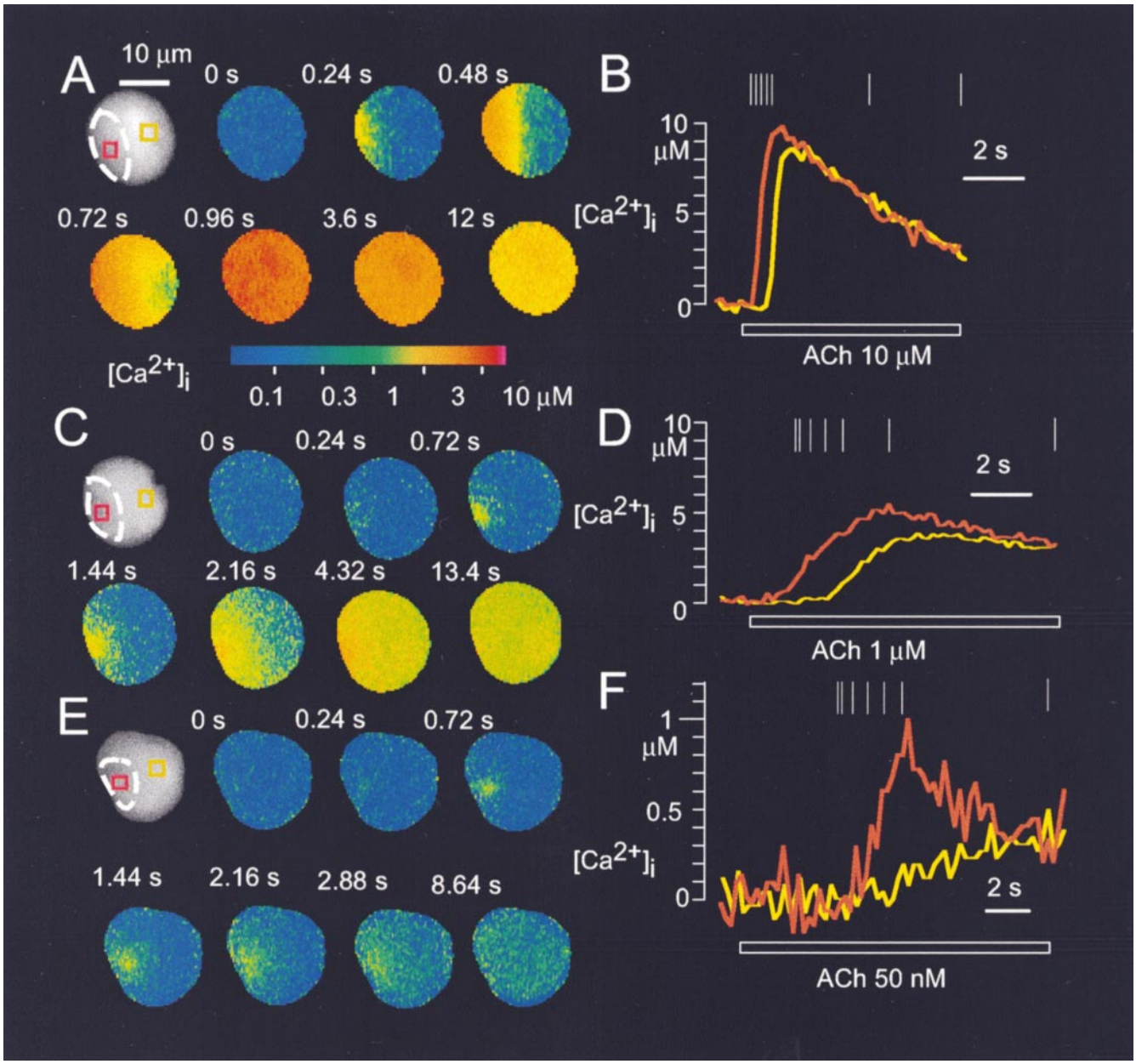

Figure 3. ACh-induced global Ca^{2+} spikes. Ca^{2+} waves induced by exposure of acinar cells to ACh at concentrations of 10 μM (A and B), 1 μM (C and D), or 50 nM (E and F) were imaged with a cooled CCD camera and BTC. The horizontal bars in (B), (D), and (F) indicate the duration of exposure to ACh.

creases in $[IP_3]_i$ can induce Ca^{2+} spikes in acinar cells that share most features of those induced by ACh, consistent with the role of IP_3 as the Ca^{2+}-mobilizing messenger for this neurotransmitter. Our data have also confirmed that subcellular gradients of IP_3 sensitivities are important for the generation of all forms of Ca^{2+} spikes in these cells, and that IP_3 is a long-range messenger and act as a global signal in those cells with diameters less than 20 μM (Allbritton et al., 1992; Kasai and Petersen, 1994). Moreover, we have shown that the temporal profile of $[IP_3]_i$ affects the kinetics of global Ca^{2+} spikes.

Control of Global Ca^{2+} Spikes by IP_3 Production

The time courses of global Ca^{2+} spikes induced by instantaneous increases in $[IP_3]_i$ were faster than those of ACh-induced Ca^{2+} spikes at all concentrations of IP_3 and ACh examined. This observation indicates that ACh-induced activation of PLC results in a gradual increase in $[IP_3]_i$, and that the kinetics of $[IP_3]_i$ is a key determinant of the time course of global Ca^{2+} spikes. Thus, we propose a mechanism for the generation of Ca^{2+} spikes in which the time course of their spread reflects that of $[IP_3]_i$, and in which their extent and amplitude are determined by the

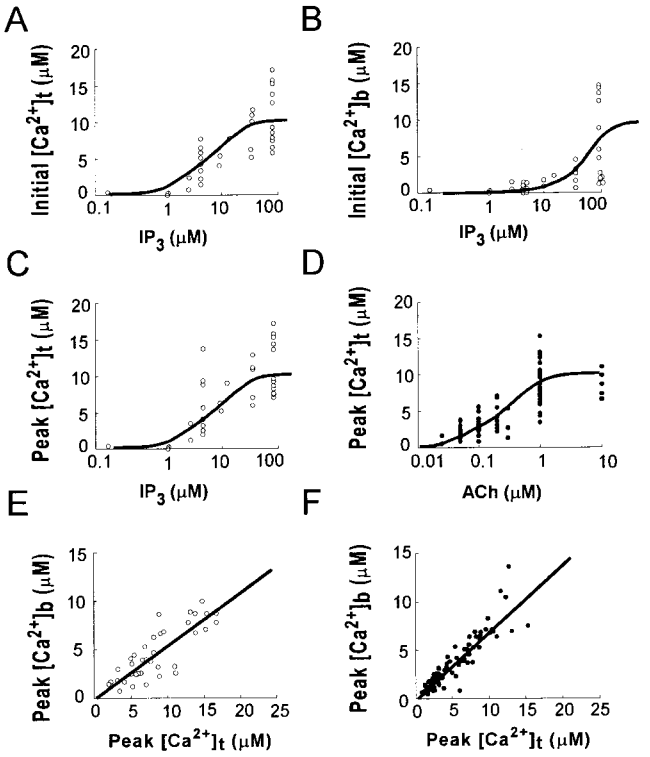

Figure 4. Dose dependence of amplitudes of global Ca^{2+} spikes induced by caged IP_3 or ACh. (A and B) Semilog plots of $[Ca^{2+}]_i$ immediately (0.24 s) after photolysis of caged IP_3 in the trigger zone ($[Ca^{2+}]_t$) (A) and in the basal area ($[Ca^{2+}]_b$) (B), respectively. The smooth curves were drawn assuming median effective concentrations of 5 and 50 μM, respectively. (C and D) Semilog plots of peak $[Ca^{2+}]_i$ in the trigger zone ($[Ca^{2+}]_t$) versus $[IP_3]_i$ (C) or ACh concentration (D). The smooth curves were drawn assuming median effective concentrations of 10 and 0.5 μM for IP_3 and ACh, respectively. (E and F) Correlations between peak $[Ca^{2+}]_i$ in the trigger zone ($[Ca^{2+}]_t$) and that in the basal area ($[Ca^{2+}]_b$) for global Ca^{2+} spikes induced by IP_3 or ACh, respectively. The regression coefficients are 0.57 and 0.63 for IP_3 and ACh, respectively.

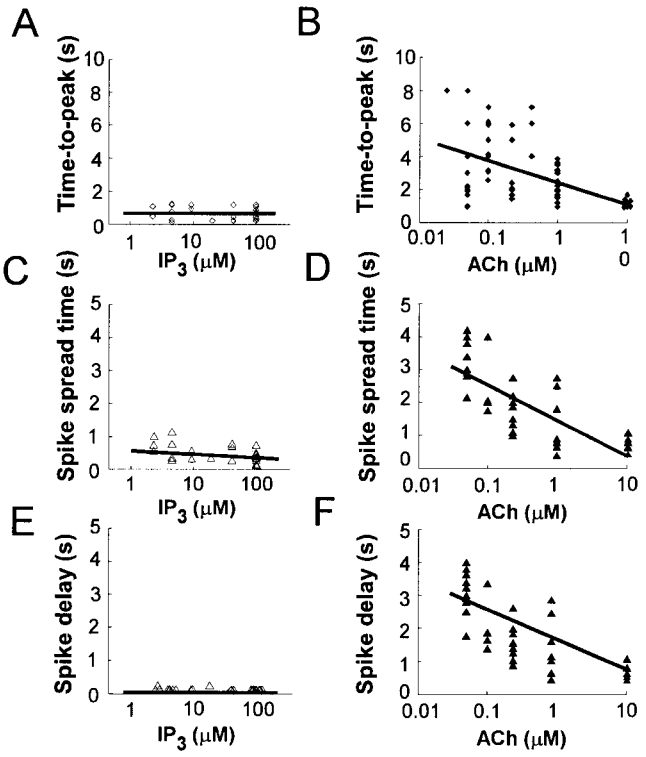

Figure 5. Dose dependence of time courses of global Ca^{2+} spikes induced by caged IP_3 or ACh. (A and B) Semilog plots of the time-to-peak of Ca^{2+} spikes in the trigger zone versus concentration of IP_3 (A) or ACh (B). (C and D) Semilog plots of spike spread time versus concentration of IP_3 (C) or ACh (D). (E and F) Semilog plots of spike delay time versus concentration of IP_3 (E) or ACh (F). Correlation coefficients are 0.066 ($P > 0.1$), 0.45 ($P < 0.001$), 0.29 ($P > 0.1$), 0.63 ($P < 0.001$), 0.003 ($P > 0.1$), and 0.61 ($P < 0.001$) for A through F, respectively.

maximal $[IP_3]_i$ (Fig. 7). The control of Ca^{2+} spikes by IP_3 production can explain simply the key properties of agonist-induced Ca^{2+} spikes in exocrine gland cells. First, the spread of Ca^{2+} spikes is relatively slow (5–15 μm/s; Kasai and Augustine, 1990; Jaffe, 1991; Toescu et al., 1992). Second, their extent and speed depend on agonist type and concentration (Fig. 5; Nathanson et al., 1992; Kasai et al., 1993; Thorn et al., 1993; Sjoedin et al., 1997; Pfeiffer et al., 1998). And finally, their amplitude varies over a large concentration range (0.5 to >10 μM) depending on the agonist concentration (Fig. 4). Thus, global Ca^{2+} spikes in acinar cells predominantly reflect global increases in $[IP_3]_i$, which are predicted to reach a maximum 1 to 8 s after the application of ACh (Fig. 5 B).

Our data also support role of CICR mechanisms of Ca^{2+} release channels in global Ca^{2+} spikes, because gradual increases in $[Ca^{2+}]_i$ were induced in response to rapid photolysis of caged IP_3 (Fig. 2, C–H). However, these increases in $[Ca^{2+}]_i$ were too fast (Fig. 5, A, C, and E) to account for ACh-induced global Ca^{2+} spikes (Fig. 5, B, D, and F). Thus, it is conceivable that the CICR mechanism locally generates Ca^{2+} spikes, and that the increases in $[IP_3]_i$ control the spread of such Ca^{2+} spikes. Since gradual increases in $[IP_3]_i$ determine the kinetics of global Ca^{2+} spikes, it is likely that the positive feedback effect of Ca^{2+} on PLC plays a role in the generation of global Ca^{2+} spikes and oscillation in acinar cells as suggested in other preparations (Meyer and Stryer, 1988; Harootunian et al., 1991; Hirose et al., 1999). In contrast, local Ca^{2+} spikes appear to be mediated solely by CICR mechanisms, because they occurred at constant level of $[IP_3]_i$ (Fig. 1; Wakui et al., 1989; Thorn et al., 1996).

Given that the production of IP_3 by PLC is not instantaneous in any cell type, the resulting time-dependent increase in $[IP_3]_i$ may be crucial to Ca^{2+} spikes in general. Moreover, long-range control of Ca^{2+} spike spread (Fig. 7) can be applied to cells in which gradients of IP_3 sensitivity exist (Inagaki et al., 1991; Fay et al., 1995; Lefevre et al., 1995; Robb-Gaspers and Thomas, 1995; Missiaen et al., 1996; Simpson et al., 1997; Callamaras et al., 1998; Yamamoto-Hino et al., 1998). Thus, mechanisms of Ca^{2+} spiking generally involve (a) PLC dependent long-range control (Fig. 7), (b) local CICR mechanisms (Berridge, 1993; Pe-

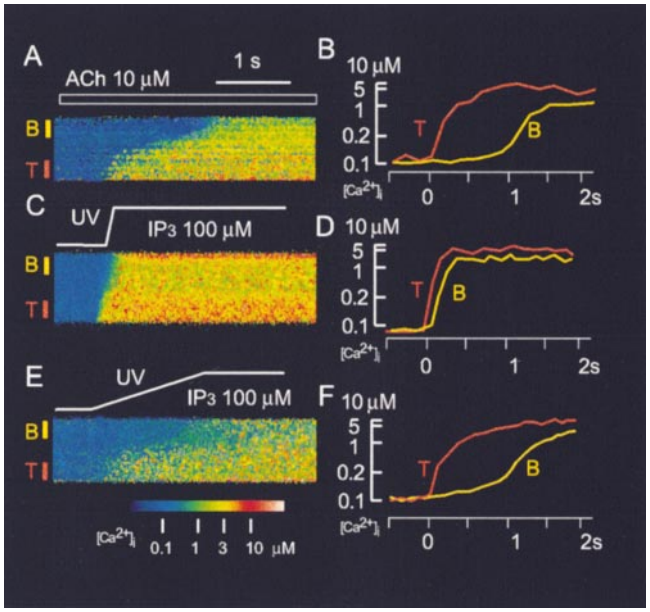

Figure 6. Line-scan analysis of global Ca^{2+} spikes induced by ACh or caged IP_3. (A, C, and E) Increases in $[Ca^{2+}]_i$ recorded with the line-scan mode of the confocal microscope and with fluo-3 as the Ca^{2+} indicator. The trigger zone and basal area of the acinar cells are denoted by T and B, respectively. The cells were stimulated either with 10 μM ACh (A), or by rapid (C) or slow (E) photolysis (indicated by tracings above images) of 100 μM caged IP_3. (B, D, and F) Time courses of $[Ca^{2+}]_i$ in the trigger zones and basal areas for the cells shown in A, C, and E, respectively.

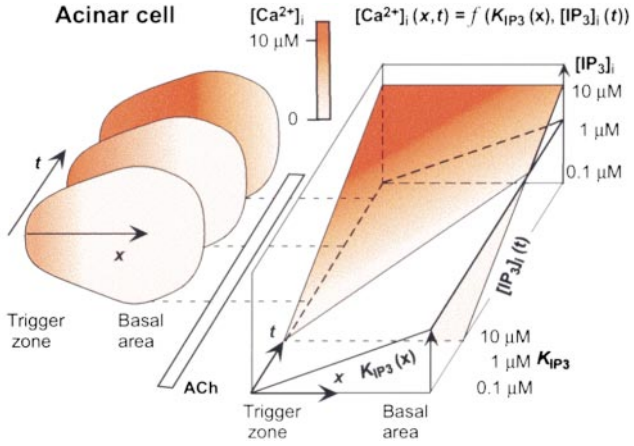

Figure 7. Control of Ca^{2+} spikes by IP_3 production in pancreatic acinar cells. Increases in $[IP_3]_i$ can trigger spread of Ca^{2+} spikes (Ca^{2+} waves) by sequential activation of IP_3 receptors, if there is a spatial gradient of IP_3 sensitivity across the cell and if the rate of IP_3 production is slower than that of the CICR-mediated Ca^{2+} spikes. For simplicity, if we assume that the CICR mechanism occurred instantaneously, the distribution of $[Ca^{2+}]_i$ is expressed as a function of the IP_3 sensitivity at a specific place, $K_{IP3}(x)$, and of $[IP_3]_i$ at a specific time, $[IP_3]_i(t)$. $[Ca^{2+}]_i$ is determined by a balance between CICR-amplified Ca^{2+} release and Ca^{2+} removal mechanisms. When $[IP_3]_i$ is small, local Ca^{2+} spikes result; when $[IP_3]_i$ is large, Ca^{2+} spikes spread further, and generate global Ca^{2+} spikes in a dose-dependent manner. More rapid increases in $[IP_3]_i$ result in a faster spread of Ca^{2+} spikes. Thus, kinetics of IP_3 production play a key role in the amplitude, extent, and time course of Ca^{2+} spikes. The same mechanism is operative in the generation of Ca^{2+} spikes in those cells with heterogenous IP_3 receptors, even though there is no spatial gradient in IP_3 receptors.

tersen et al., 1994; Clapham, 1995), and (c) heterogeneity in the Ca^{2+} release channels.

Types of IP_3 Receptors

The control of global Ca^{2+} spikes by $[IP_3]_i$ in pancreatic acinar cells is consistent with the previous observation that agonists and IP_3 each mobilize Ca^{2+} in a dose-dependent manner (Muallem et al., 1989; Petersen et al., 1991a,b). Our data further demonstrate that such dose-dependent control involves heterogeneity in the Ca^{2+}-release processes distributed in various subcellular regions and results in a wide range of $[Ca^{2+}]_i$ (0.1 to >10 μM). The graded nature of Ca^{2+} spikes (Fig. 4, C and D) may reflect the balance between Ca^{2+} release and clearance in vivo (van de Put et al., 1994).

It has reported that all three types of IP_3 receptors were expressed in acinar cells (Lee et al., 1997). The presence of type-1 IP_3 receptors may account for the initiation of Ca^{2+} spikes and oscillations in the trigger zone (Hagar et al., 1998; Miyakawa et al., 1999). The preferential localization of type-3 IP_3 receptors in the trigger zone (Nathanson et al., 1994) is possibly responsible for the large increases in $[Ca^{2+}]_i$ in this region, given the small inhibitory effect of Ca^{2+} on these receptors (Hagar et al., 1998). It is therefore suggested that the type-3 IP_3 receptor plays a specific role in cellular processes such as exocytosis that require high $[Ca^{2+}]_i$ (Ito et al., 1997; Kasai and Takahashi, 1999). The Ca^{2+} release in the trigger zone exhibited a similar sensitivity (Fig. 4 A) to the type-3 IP_3 receptors in vivo (Miyakawa et al., 1999). The reasons for 10 times lower IP_3 sensitivity in the basal area (Fig. 4 B) remain to be clarified.

Acinar cells may differ from oocytes and smooth muscle cells in that the latter cell types express predominantly one type of IP_3 receptor, and Ca^{2+} spikes in these cells occur in an all-or-nothing manner (Lechleiter and Clapham, 1992; Parker and Ivorra, 1993; Iino et al., 1993). Thus, the distributions of distinct IP_3 receptors appear critical for Ca^{2+}-dependent cellular functions.

We thank T. Kishimoto, A. Tachikawa, H. Maeda, and T. Nemoto for collaboration throughout the experiments, M. Iino and K. Hirose for helpful discussions, and M. Ogawa for technical assistance.

This work was supported by the Research for the Future program of the Japan Society for the Promotion of Science (JSPS), grants-in-aid from the Ministry of Education, Science, and Culture of Japan, a research grant from the Human Frontier Science Program, a grant from the Toyota Foundation, and CREST (Core Research for Evolutional Science and Technology) of the Japan Science and Technology Corporation (JST). K. Ito is a research fellow of JSPS, and is now at School of Life Science, Tokyo University of Pharmacy and Life Science, Hachiooji, Tokyo 192-0392.

Received: 29 March 1999
Revised: 10 June 1999
Accepted: 15 June 1999

References

Allbritton, N.L., T. Meyer, and L. Stryer. 1992. Range of messenger action of calcium ion and inositol 1,4,5-trisphosphate. *Science*. 258:1812–1815.

Berridge, M.J. 1993. Inositol trisphosphate and calcium signaling. *Nature*. 361: 315–325.

Bezprozvanny, I., J. Watras, and B.E. Ehrlich. 1991. Bell-shaped calcium-response curves of Ins(1,4,5)P_3- and calcium-gated channels from endoplasmic reticulum of cerebellum. *Nature*. 351:751–754.

Bootman, M.D., M.J. Berridge, and P. Lipp. 1997. Cooking with calcium: the recipes for composing global signals from elementary events. *Cell*. 91:367–373.

Callamaras, N., J.S. Marchant, X.P. Sun, and I. Parker. 1998. Activation and coordination of InsP3-mediated elementary Ca^{2+} events during global Ca^{2+} signals in *Xenopus* oocytes. *J. Physiol*. 509:81–91.

Clapham, D.E. 1995. Calcium signaling. *Cell*. 80:259–268.

Endo, M., M. Tanaka, and Y. Ogawa. 1970. Calcium induced release of calcium from the sarcoplasmic reticulum of skinned skeletal muscle fibres. *Nature*. 228:34–36.

Fay, F.S., S.H. Gilbert, and R.A. Brundage. 1995. Calcium signaling during chemotaxis. *Ciba Found. Symp*. 188:121–135.

Hagar, R.E., A.D. Burgstahler, M.H. Nathanson, and B.E. Ehrlich. 1998. Type III InsP(3) receptor channel stays open in the presence of increased calcium. *Nature*. 396:81–84.

Harootunian, A.T., J.P. Kao, S. Paranjape, and R.Y. Tsien. 1991. Generation of calcium oscillations in fibroblasts by positive feedback between calcium and IP_3. *Science*. 251:75–78.

Hirose, K., S. Kadowaki, M. Tanabe, H. Takeshima, and M. Iino. 1999. Spatiotemporal dynamics of inositol 1,4,5-trisphosphate that underlies complex Ca^{2+} mobilization patterns. *Science*. 284:1527–1530.

Iino, M. 1989. Calcium-induced calcium release mechanism in guinea pig taenia caeci. *J. Gen. Physiol*. 94:363–383.

Iino, M., T. Yamazawa, Y. Miyashita, M. Endo, and H. Kasai. 1993. Critical intracellular Ca^{2+} concentration for all-or-none Ca^{2+} spiking in single smooth muscle cells. *EMBO (Eur. Mol. Biol. Organ.) J*. 12:5287–5291.

Inagaki, N., H. Fukui, S. Ito, A. Yamatodani, and H. Wada. 1991. Single type-2 astrocytes show multiple independent sites of Ca^{2+} signaling in response to histamine. *Proc. Natl. Acad. Sci. USA*. 88:4215–4219.

Ito, K., Y. Miyashita, and H. Kasai. 1997. Micromolar and submicromolar Ca^{2+} spikes regulating distinct cellular functions in pancreatic acinar cells. *EMBO (Eur. Mol. Biol. Organ.) J*. 16:242–251.

Jaffe, L.F. 1991. The path of calcium in cytosolic calcium oscillations: a unifying hypothesis. *Proc. Natl. Acad. Sci. USA*. 88:9883–9887.

Kasai, H., and G.J. Augustine. 1990. Cytosolic Ca^{2+} gradients triggering unidirectional fluid secretion from exocrine pancreas. *Nature*. 348:735–738.

Kasai, H., and O.H. Petersen. 1994. Spatial dynamics of second messengers: IP_3 and cAMP as long-range and associative messengers. *Trends Neurosci*. 17: 95–101.

Kasai, H., and N. Takahashi. 1999. Multiple kinetic components and the Ca^{2+} requirements of exocytosis. *Philos. Trans. R. Soc. Lond. Ser. B Biol. Sci*. 354: 331–335.

Kasai, H., Y. Li, and Y. Miyashita. 1993. Subcellular distribution of Ca^{2+} release channels underlying Ca^{2+} waves and oscillations in exocrine pancreas. *Cell*. 74:669–677.

Lechleiter, J.D., and D.E. Clapham. 1992. Molecular mechanisms of intracellular calcium excitability in *X. laevis* oocytes. *Cell*. 69:283–294.

Lee, M.G., X. Xu, W. Zeng, J. Diaz, R.J.H. Wojcikiewicz, T.H. Kuo, F. Wuytack, L. Racymaekers, and S. Muallem. 1997. Polarized expression of Ca^{2+} channels in pancreatic and salivary gland cells. *J. Biol. Chem*. 272: 15765–15770.

Lefevre, B., A. Pesty, and J. Testart. 1995. Cytoplasmic and nucleic calcium oscillations in immature mouse oocytes: evidence of wave polarization by confocal imaging. *Exp. Cell Res*. 218:166–173.

Maruyama, Y., G. Inooka, Y. Li, Y. Miyashita, and H. Kasai. 1993. Agonist-induced localized Ca^{2+} spikes directly triggering exocytotic secretion in exocrine pancreas. *EMBO (Eur. Mol. Biol. Organ.) J*. 12:3017–3022.

Meyer, T., and L. Stryer. 1988. Molecular model for receptor-stimulated calcium spiking. *Proc. Natl. Acad. Sci. USA*. 85:5051–5055.

Missiaen, L., F.X. Lemaire, J.B. Parys, H. De Smedt, I. Sienaert, and R. Casteels. 1996. Initiation sites for Ca^{2+} signals in endothelial cells. *Pflugers Arch*. 431:318–324.

Miyakawa, T., A. Maeda, T. Yamazawa, K. Hirose, T. Kurosaki, and M. Iino. 1999. Encoding of Ca^{2+} signals by differential expression of IP_3 receptor subtypes. *EMBO (Eur. Mol. Biol. Organ.) J*. 18:1303–1308.

Muallem, S., S.J. Pandol, and T.G. Beeker. 1989. Hormone-evoked calcium release from intracellular stores is a quantal process. *J. Biol. Chem*. 264:205–212.

Nathanson, M.H., P.J. Padfield, A.J. O'Sullivan, A.D. Burgstahler, and J.D. Jamieson. 1992. Mechanism of Ca^{2+} wave propagation in pancreatic acinar cells. *J. Biol. Chem*. 267:18118–18121.

Nathanson, M.H., M.B. Fallon, P.J. Padfield, and A.R. Maranto. 1994. Localization of the type 3 inositol 1,4,5-trisphosphate receptor in the Ca^{2+} wave trigger zone of pancreatic acinar cells. *J. Biol. Chem*. 269:4693–4696.

Parker, I., and I. Ivorra. 1993. Confocal microfluorimetry of Ca^{2+} signals evoked in *Xenopus* oocytes by photoreleased inositol trisphosphate. *J. Physiol*. 461:133–165.

Petersen, O.H. 1992. Stimulus-secretion coupling: cytoplasmic calcium signals and the control of ion channels in exocrine acinar cells. *J. Physiol*. 448:1–51.

Petersen, C.C., E.C. Toescu, and O.H. Petersen. 1991a. Different patterns of receptor-activated cytoplasmic Ca^{2+} oscillations in single pancreatic acinar cells: dependence on receptor type, agonist concentration and intracellular Ca^{2+} buffering. *EMBO (Eur. Mol. Biol. Organ.) J*. 10:527–533.

Petersen, C.C., E.C. Toescu, B.V. Potter, and O.H. Petersen. 1991b. Inositol triphosphate produces different patterns of cytoplasmic Ca^{2+} spiking depending on its concentration. *FEBS Lett*. 293:179–182.

Petersen, O.H., C.C.H. Petersen, and H. Kasai. 1994. Calcium and hormone action. *Annu. Rev. Physiol*. 56:297–319.

Pfeiffer, F., L. Sternfeld, A. Schmid, and I. Schulz. 1998. Control of Ca^{2+} wave propagation in mouse pancreatic acinar cells. *Am. J. Physiol*. 274:C663–C672.

Robb-Gaspers, L.D., and A.P. Thomas. 1995. Coordination of Ca^{2+} signaling by intercellular propagation of Ca^{2+} waves in the intact liver. *J. Biol. Chem*. 270:8102–8107.

Simpson, P.B., S. Mehotra, G.D. Lange, and J.T. Russell. 1997. High density distribution of endoplasmic reticulum proteins and mitochondria at specialized Ca^{2+} release sites in oligodendrocyte processes. *J. Biol. Chem*. 272: 22654–22661.

Sjoedin, L., K. Ito, Y. Miyashita, and H. Kasai. 1997. Cytoplasmic Ca^{2+} gradients evoked by acetylcholine and peptides in pancreatic acinar cells of the guinea pig. *Pflugers Archiv*. 433:397–402.

Thorn, P., A.M. Lawrie, P.M. Smith, D.V. Gallacher, and O.H. Petersen. 1993. Local and global Ca^{2+} oscillations in exocrine cells evoked by agonists and inositol trisphosphate. *Cell*. 74:661–668.

Thorn, P., R. Moreton, and M. Berridge. 1996. Multiple, coordinate Ca^{2+}-release events underlie the inositol trisphosphate-induced local Ca^{2+} spikes in mouse pancreatic acinar cells. *EMBO (Eur. Mol. Biol. Organ.) J*. 15:999–1003.

Toescu, E.C., A.M. Lawrie, O.H. Petersen, and D.V. Gallacher. 1992. Spatial and temporal distribution of agonist-evoked cytoplasmic Ca^{2+} signals in exocrine cells analysed by digital image microscopy. *EMBO (Eur. Mol. Biol. Organ.) J*. 11:1623–1629.

van de Put, F.H., J.J. De Pont, and P.H. Willems. 1994. Heterogeneity between intracellular Ca^{2+} stores as the underlying principle of quantal Ca^{2+} release by inositol 1,4,5-trisphosphate in permeabilized pancreatic acinar cells. *J. Biol. Chem*. 269:12438–12443.

Wakui, M., B.V. Potter, and O.H. Petersen. 1989. Pulsatile intracellular calcium release does not depend on fluctuations in inositol trisphosphate concentration. *Nature*. 339:317–320.

Yamamoto-Hino, M., A. Miyawaki, A. Segawa, E. Adachi, S. Yamashina, T. Fujimoto, T. Sugiyama, T. Furuichi, M. Hasegawa, and K. Mikoshiba. 1998. Apical vesicles bearing inositol 1,4,5-trisphosphate receptors in the Ca^{2+} initiation site of ductal epithelium of submandibular gland. *J. Cell Biol*. 141: 135–142.